Measurement by digital image correlation of the topography of a liquid interface

Frederic Moisy, Marc Rabaud, E Pinsolle

MEASUREMENT BY DIGITAL IMAGE CORRELATION OF THE TOPOGRAPHY OF A LIQUID INTERFACE

F. Moisy, M. Rabaud, E. Pinsolle
University Paris-Sud; University Pierre et Marie Curie ; CNRS.
Fluides, Automatiques et Systemes Thermiques (FAST),
Batiment 502, Campus Universitaire, F-91405 Orsay, France.

KEYWORDS:
Main subject(s): *Free surface measurement, water waves*
Visualization method(s): *Refractometry, image correlation, synthetic schlieren*

ABSTRACT : *A non intrusive optical method for an accurate measurement of the instantaneous topography of the interface between two transparent fluids is characterized. This method is based on the analysis of the refracted image of a random dot pattern visualized through the interface. The apparent displacement field between the refracted image and a reference image obtained when the surface is flat is determined using a Digital Image Correlation (DIC) algorithm. A numerical integration of this displacement field, based on a least square inversion of the gradient operator, is used for the reconstruction of the instantaneous surface height, allowing for an excellent spatial resolution with a low computational cost. The main limitation of the method, namely the ray crossing (caustics) due to strong curvature and/or large surface-pattern distance, is discussed. Two examples of applications illustrate this method: The time-resolved observation of the circular waves generated by a water drop impact, and the dynamical wetting of a drop on a glass substrate.*

1 Introduction

The measurement of the deformation of a liquid surface is of fundamental and practical interest in a number of applications, from small scales (e.g. painting or coating industry) to large scales (e.g. wind waves, ship wakes). Optical methods, being non intrusive and able to provide instantaneous two-dimensional measurements, are of much practical interest. Measurements based on the use of collimated light beam encoded with a linearly increasing intensity (for one component) or color-encoded (for two components) have been proposed [1,2]. From those measurements, the surface elevation could be obtained by integration of the gradient components in the Fourier domain. The main advantage of using collimated light is that the measured gradient is insensitive to the surface height. However, the drawback is the need for large lenses to produce a collimated beam of the size of the imaged surface area. Roesgen et al. [3] introduced a new approach, also based on collimated light, using an array of microlenses placed above the free surface. The surface deformation leads to a displacement of the light spots in the focal plane of the microlens array, which could be measured using a Digital Image Correlation (DIC) algorithm. Here again, the size of the microlens array limits the size of the imaged area, restricting this approach to small fields.

Another image-encoding approach, first discussed by Kurata et al. [4], relies on the use of scattered light emitted from a structured pattern, usually a grating or a set of random dots, imaged through the interface. Here the displacement field is obtained by comparing the refracted images of the pattern obtained with flat and deformed surfaces. Using scattered light instead of collimated light allows for simplification of the optical setup, since no collimating lens is needed, but the resulting measurement is a combination the surface slope and height. This approach has been mainly applied to measurements in stratified fluids, in the so-called synthetic Schlieren or background-oriented Schlieren (BOS) methods [5,6], using again a DIC algorithm for the computation of the displacement field. Elwell [7] successfully used this idea to obtain quantitative measurements of the surface deformation induced by vortices in a shallow water flow, using a cumulative sum scheme of the measured gradient components for the surface height reconstruction.

This paper presents a detailed characterization of the method originally introduced by Kurata et al. [4], offering an accurate and low-cost measurement of the instantaneous topography of the interface between two transparent fluids [8]. We show that a precision of 1 μm for a 10 cm field can be readily achieved, making this method attractive for investigation of small-scale waves dynamics or coating phenomena. The method consists in two steps: (i) measurement of the surface gradient from the displacement field of the refracted image of a random pattern using a Digital Image Correlation (DIC) algorithm; (ii) reconstruction of the surface height, using a least-square integration of the surface gradient. Compared to the other cited methods, which require an elaborate optical setup and a delicate calibration scheme, the method described here is simply based on a standard black-and-white imaging system with no specific optics. As a consequence it may be easily reproduced for a large range of applications using standard laboratory equipment. The drawback of this simplified setup is that, since no collimating optics is used, oblique light rays have to be considered, yielding to a more delicate analysis of the ray geometry in the general case. It can be shown however that, to first order in paraxial angles, in surface slopes, and in relative deformations, the surface gradient is simply related to the displacement field [8].

The computation of the displacement field from the refracted images of the flat and deformed interface is based on a standard DIC algorithm. Due to its wide use in solid and fluid mechanics, DIC algorithms have received considerable interest in recent years, and several commercial and open-source packages are now available. DIC algorithms are routinely used in Particle Image Velocimetry (PIV) applications, where the velocity field is given by the displacement field of tracer particles per unit of sampling time [9]. The second step of the method, the integration of the gradient field, is based on a least-square inversion of the gradient operator, here again available from standard linear algebra packages.

2 Relation between the surface gradient and the displacement field

We want to determine the optical displacement field $\delta\mathbf{r}\ (x,y)$ induced by the refraction of the light scattered from a pattern located at $z = 0$ through the interface $z = h(x,y)$. At each object point M of the pattern, we need to determine the virtual objects M' and M'' corresponding to the flat and deformed interface respectively, and to relate the displacement $\mathbf{M'M''} = \delta\mathbf{r}$ with the surface gradient ∇h at the same point. We consider here only the case where the camera is located above the free surface. The refraction indices of the upper and lower fluids are noted n and n' respectively. With $n' > n$, wave

crests and troughs will act as magnifying (convex) and reducing (concave) lenses. For the sake of simplicity, the pattern-surface distance h_p is first chosen equal to the liquid depth h_0.

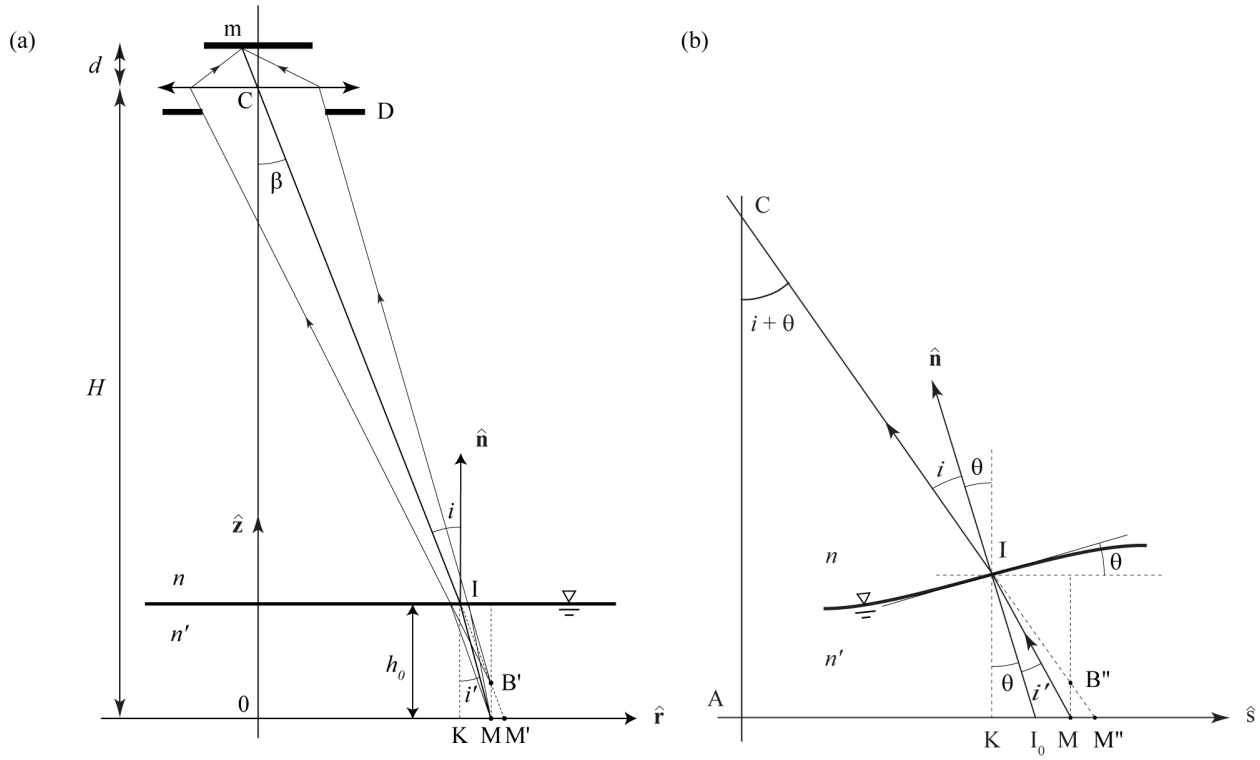

Fig. 1. Virtual objects M' and M'' associated to an object M, for (a) the flat surface, and (b) the deformed surface. Note that, in (b), the incidence plane is not vertical.

We first consider the refracted image of the pattern at $z = 0$ through a flat interface at $z = h_p$ (Fig.1a). A point M located in (x_M, y_M, 0) has its virtual object B' located above the pattern, in (x_M, y_M, αh_p), with $\alpha = 1 - n/n'$. Since rays reaching the image plane appear to come from a point M' in the pattern plane, in the following the apparent displacements are simply given in the plane $z = 0$. The Snell-Descarte law, for small incidence angles, $ni = n'i'$, gives

$$\mathbf{MM'} = \alpha\, h_p\, i\, \mathbf{r} / |\mathbf{r}| \qquad (1)$$

We consider now the refracted image of the pattern through an arbitrary deformed interface, and we want to determine the new virtual object M'' associated to the object point M (Fig. 1b). This problem is more delicate in general, since now the incidence plane is not vertical (except for axisymmetric deformations), and does not contain the optical axis z. The incidence plane is now defined as the plane containing M, the camera C, and the unit vector $\mathbf{n}$, and intercepts the pattern plane along the direction $\mathbf{s} = \mathbf{OM} / H - \nabla h$. The displacement $\mathbf{MM''}$ is along $\mathbf{s}$, and is given by

$$\mathbf{MM''} = \alpha\, h_p\, i\, \mathbf{s} / |\mathbf{s}| \qquad (2)$$

For a camera far above the surface ($H >> L$), except for weak slopes, **s** tends to be along the surface gradient. Finally, expressed in terms of the displacement $\delta\mathbf{r} = \mathbf{M'M''}$ only, the surface gradient writes

$$\nabla \boldsymbol{h} = -\delta\mathbf{r} / h^*, \quad \text{with} \quad 1/h^* = 1/\alpha h_p - 1/H > 0 \tag{3}$$

In practice, with a camera far above the imaged surface, $H >> h_p$, we can simply consider $h^* = \alpha h_p$. If one or more intermediate materials (e.g. a glass plate) are also present between the lower fluid and the pattern, the distance h_p should be replaced by the sum of the thicknesses weighted by their respective refraction indices.

Note that it is implicitly assumed here that the displacement field $\delta\mathbf{r}$ could be determined from the refracted image of the pattern. However, this is not true if crossings of light rays occur between the pattern and the interface, which would result in the formation of caustics. To avoid this, the focal length associated to the surface curvature has to be larger than the surface-pattern distance everywhere in the imaged field. For example, in the case of a sinusoidal plane wave of amplitude η_0 and wavelength λ, ray crossings are avoided by choosing a surface-pattern distance smaller than the critical distance $h_{p,c}$,

$$h_p < h_{p,c} = \lambda^2 / (4\,\pi^2\,\alpha\,\eta_0) \tag{4}$$

Satisfying the condition for no ray crossing for arbitrary direction requires that the largest (extensional) strain remains everywhere bounded by 1. Denoting $\sigma_1 < \sigma_2$ the two ordered principal strains (these are the eigenvalues of the strain tensor $d\delta r_i / dx_j$), caustics are avoided if $\sigma_2 < 1$ at each point of the field. This is clearly an *a posteriori* test, since the computation of the principal strains requires the displacement field to be determined. However, the measurement of the principal strains provides an interesting test of *how far* the light rays are from crossing.

3 Experimental results

3.1 Experimental setup

Two series of experiments have been performed: visualization of the wave pattern generated by the impact of a water drop, and visualization of the spreading of a silicon oil drop on a glass substrate. The setup for the first experiment, using a 60 cm x 40 cm glass tank filled with water up to a height $h_0 = 4$ cm, is shown in Fig 2, with an example of random dot pattern. The pattern has been carefully designed to allow for unambiguous reconstruction of the displacement field with a good spatial resolution. The camera resolution and the expected displacement magnitude have to be taken into account to optimize the characteristic size of the fine structure of the pattern. In order to maximize the quantity of information and to reduce fortuitous coincidences, a set of randomly distributed dots, partially overlapping, is used. Best results for cross-correlation algorithms are obtained when the diameter of the dots corresponds to 2-3 pixels [9]. In this example, dots of diameter 0.4 mm, made of concentric circles of increasing grayscale, have been numerically generated and printed on an overhead transparency.

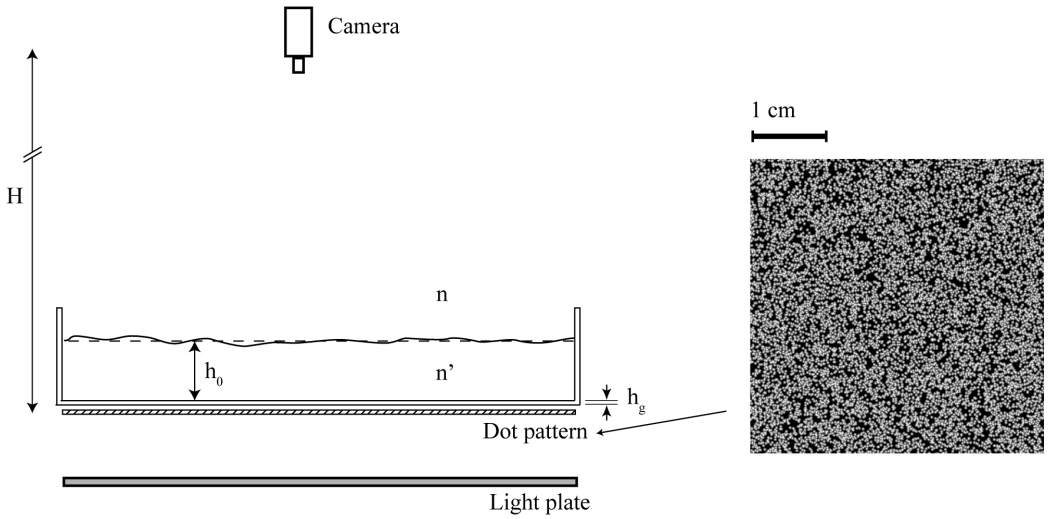

Fig. 2. Experimental setup and example of random dot pattern.

3.2 Displacement field computation

The displacement field $\delta\mathbf{r}(x,y)$ between each image and the reference image is obtained by the DIC algorithm available in the commercial software DaVis [10]. Interrogation windows of size 16x16 pixels, with 50% overlap, are used for the computations of the correlation functions. The dots size and density have been adjusted to give a mean number of 5 dots per interrogation window. For a 2048x2048 pixels camera, the final displacement field is defined on a 256x256 grid, with a spatial resolution of order 0.5 mm. Classical post-processing schemes are applied, such as median filter to remove bad vectors. Since the random dot pattern is generated to meet the requirements for an optimal cross-correlation resolution, one may expect to reach the theoretical resolution of this method [9]. Using interrogation windows of decreasing size, with final size of 16x16 pixels, a resolution of 0.1 pixel (about 7 µm) can be achieved using a classical subpixel interpolation scheme. For typical displacement of order 5 pixels, and assuming moderate strain so that the dots remain essentially circular, this relative uncertainty is about 2%. Larger values may however be expected when the refracted pattern is significantly strained.

3.3 Surface height reconstruction

The numerical integration of the surface height field $h(x,y)$ from the displacement field is performed by a numerical inversion of the linear system built from the second-order centered difference gradient operator. Since the measured gradient is defined on a MxN grid, this linear system has $2MN$ equations and MN unknown. A solution may however be defined for this over-determined linear system: the resulting surface height $h(x,y)$ is the ``best" solution in the least-square sense. Being non local, the least-square solution is robust to localized bad vectors. This method is suitable for square or rectangular areas, but may be delicate to implement for more complex geometries. A strong limitation of this method is its inability to detect changes of the mean surface height, originating for example from waves of characteristic length of the order or larger than the imaged area. The integration method being linear, the relative uncertainty of the surface height reconstruction is expected to depend linearly upon the uncertainty of the input displacement field.

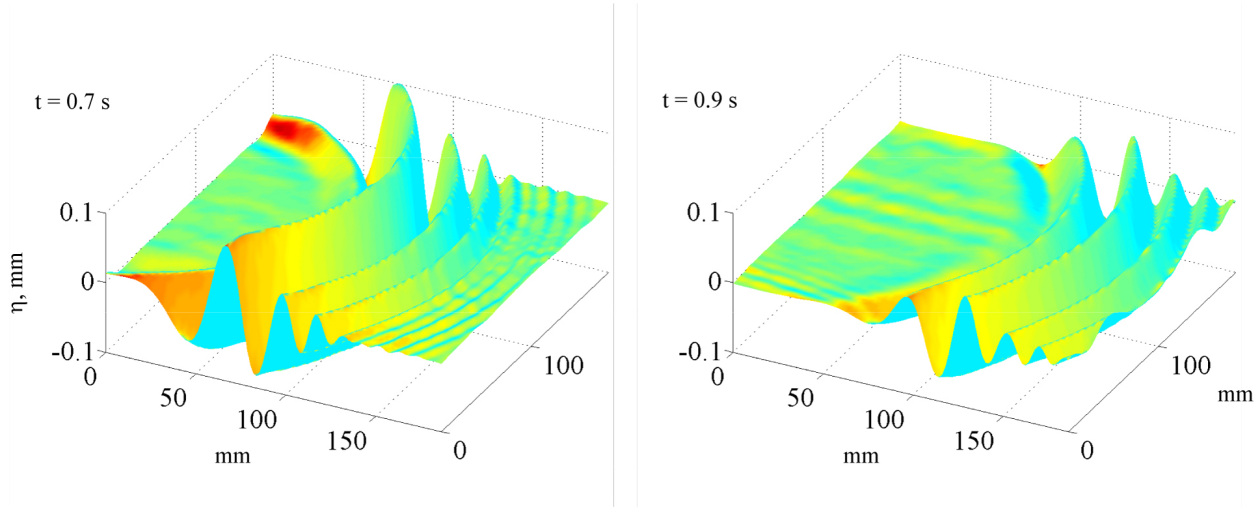

Fig. 3: Perspective view of the circular waves created by the impact of a water drop in water, at times $t = 0.7$ and $t = 0.9$ s after the impact.

3.4 Experiments of water drop impact

Time-resolved visualizations of the circular wave pattern generated by the impact of a water drop have been carried out. A water drop of 1 mm diameter is dropped one centimeter above a 4 cm water layer, and the surface height is reconstructed using a 1024x1024 camera operating at 100 Hz. The camera is located at a distance $H = 2$ m above the tank and the imaged area is a square of side 20 cm. The surface field could be measured only 0.4 s after the impact.

The two perspective views of the surface elevation in Fig. 3 clearly show the growing circular wave packet. The largest waves have amplitude of 100 µm and wavelength of order of 30 mm, but much smaller waves, of amplitude of 1 µm and wavelength around 10 mm, can also be distinguished at the front of the wave packet. Shortly after the impact, the surface near the impact is almost perfectly flat, showing only residual plane waves of amplitude less than 1 µm originating from slight background vibrations from the lateral tank walls.

3.4 Experiments of spreading of a silicon oil drop

The spreading of a liquid drop on a transparent substrate has also been investigated using this method. An experiment has been carried out, using a glass plate of 10 mm thickness placed on the random dot pattern. A 14 mm^3 drop of silicon oil, of viscosity 500 mPa s, spreads over the glass plate, and images on a 4.5x4.5 cm^2 area are acquired by a 2048x2048 camera during 3000 s at a rate of 0.1 Hz. The thickness of the glass plate is chosen large compared to the drop height, in order to satisfy the small deviation hypothesis. A view of the reconstructed drop after 800 s is shown in Fig. 4a. At that time, the radius is 5.6 mm and the height is 220 µm. The surface slope along the contact line is 0.12, a value which ensures the validity of the small slope approximation for the surface height reconstruction.

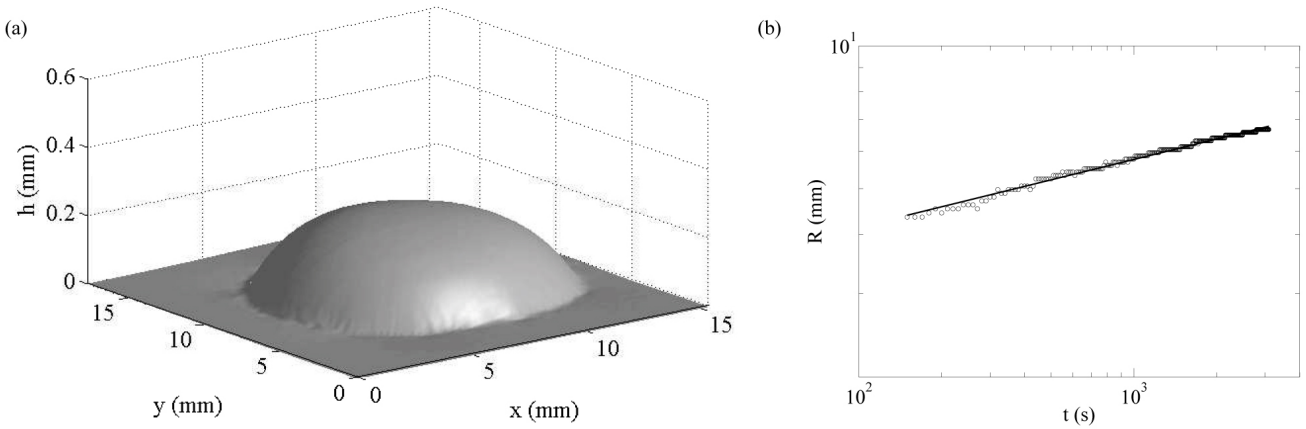

Fig. 4. (a) Perspective view of a silicon oil drop spreading on a glass plate at time t = 800 s. (b) Drop radius as a function of time. The solid line is a best fit with a power law, $R(t) \sim t^{0.14}$.

Fig. 4b shows the time evolution of the drop radius, determined here as the location where the drop surface is above 10 µm. The radius shows a well defined power law behavior, with an exponent 0.14 ± 0.01, which is close to the classical values for a spreading regime governed by the viscosity and gravity forces (exponents 1/7 or 1/8, see e.g. [11]). This observation illustrates the potential of this method for the investigation of wetting phenomena.

4 Conclusion

In this paper a low-cost and versatile optical method for an accurate measurement of the topography of an interface between two transparent fluids is characterized [8]. This method is based on the analysis of the refracted image of a random dot pattern. This non intrusive method gives quantitative measurement with a vertical resolution of order of 2%. The numerical reconstruction of the surface height, being based on a least square inversion of the gradient operator, is very robust and has a low computational cost. The main limitations of the method are: (i) it is not able to detect changes in the mean surface height; (ii) it is extremely sensitive to slight vibrations (iii) It is unable to determine the displacement field for strong curvature and/or large surface-pattern distance. Note that the limitation (ii) can be circumvented by subtracting the mean displacement field before numerical integration. However, this subtraction prevents from measuring mean surface slopes of characteristic scale of the order or larger than the imaged area. The two applications presented here demonstrate the large scope of applicability of this technique, ranging from spreading and wetting phenomena, capillary and gravity waves, and turbulence with free surface interaction.

References

1. Zhang X, Cox C S. Measuring the two-dimensional structure of a wavy water surface optically: A surface gradient detector, *Exp. Fluids*, Vol. 7, pp 225—237, 1994.
2. Zhang X, Dabiri D, Gharib M. Optical mapping of fluid density interfaces: Concepts and implementations, *Rev. Sci. Instrum*, Vol. 67, No. 5, pp 1858—1868, 1996.

3. Roesgen T, Lang A, Gharib M. Fluid surface imaging using microlens arrays, *Exp. Fluids*, Vol. 25, pp 126, 1998.
4. Kurata J, Grattan K T V, Uchiyama H, Tanaka T. Water surface mesurement in a shallow channel using the transmitted image of a grating, *Rev. Sci. Instrum.* Vol. 61, No. 2, p 736, 1990.
5. Dalziel S B, Hughes G O, Sutherland B R. Whole-field density measurements by "synthetic Schlieren", *Exp. Fluids*, Vol. 28, pp 322—335, 2000.
6. Meier G E A. Computerized background-oriented Schlieren, *Exp. Fluids*, Vol. 33, p 181, 2002.
7. Elwell F C. Flushing of Embayments, PhD thesis, University of Cambridge, 2004.
8. Moisy F, Rabaud M, Salsac K. Measurement by Digital Image Correlation of the topography of a liquid interface, submitted to *Exp. Fluids*, 2008.
9. Raffel M, Willert C E, Kompenhans J. Particle Image Velocimetry: a practical guide, Springer-Verlag, 1998.
10. DaVis, by LaVision GmbH, Anna-Vandenhoeck-Ring 19, 37081 Goettingen, Germany, complemented with the PIVMat toolbox for Matlab, http://www.fast.u-psud.fr/pivmat.
11. Bonn D, Eggers J, Indekeu J, Meunier J, Rolley E. Wetting and spreading, *Rev. Mod. Phys.*, 2008, in press.

Copyright Statement